Supplementary Information:

Multinuclear solid-state NMR investigation of structurally diverse low-dimensional hybrid metal halide perovskites

Thomas J. N. Hooper, [*a] Benny Febriansyah,[b,c] Thirumal Krishnamoorthy,[d] Walter P. D Wong,[d] Kai Xue,[e] Joel W. Ager,[b,f] Nripan Mathews [c,d]

[a.] *Centre for Membrane Separations, Adsorption, Catalysis and Spectroscopy for Sustainable Solutions (cMACS), Department of Microbial and Molecular Systems (M2S), KU Leuven, Belgium 3001.*
[b.] *Berkeley Educational Alliance for Research in Singapore (BEARS), 1 CREATE Way, Singapore 138602, Singapore.*
[c.] *Energy Research Institute at NTU (ERI@N), Research Techno Plaza, X-Frontier Block Level 5, 50 Nanyang Drive, Singapore 637553.*
[d.] *School of Materials Science and Engineering, Nanyang Technological University, 50 Nanyang Avenue, Singapore 639798, Singapore.*
[e.] *Centre of High Field Nuclear Magnetic Resonance (NMR) Spectroscopy and Imaging, Nanyang Technological University 21 Nanyang Link, Singapore 637371, Singapore.*
[f.] *Department of Materials Science and Engineering, University of California at Berkeley, Berkeley, California 94720, USA*
** Corresponding author. Email: thomas.hooper@kuleuven.be*

Table of contents

I. Supplementary figures

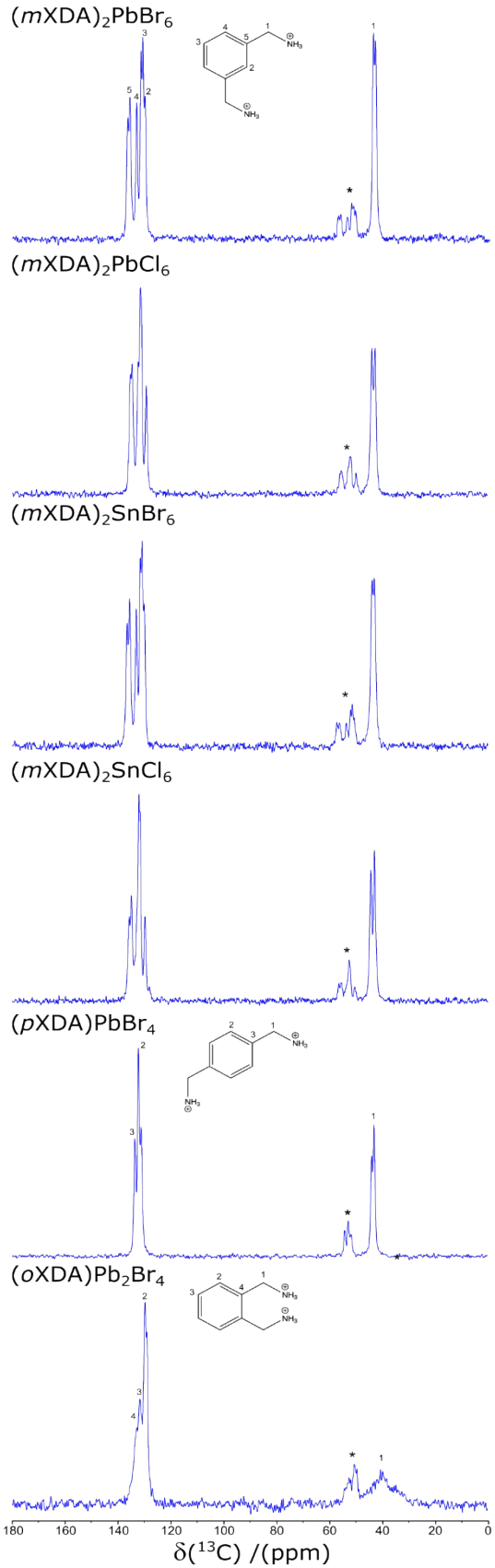

Figure S1. The ^{13}C NMR spectra of all XDA metal halide perovskites in this study, with organic cation insets detailing ^{13}C assignments. Spinning sidebands are marked by asterisks (*).

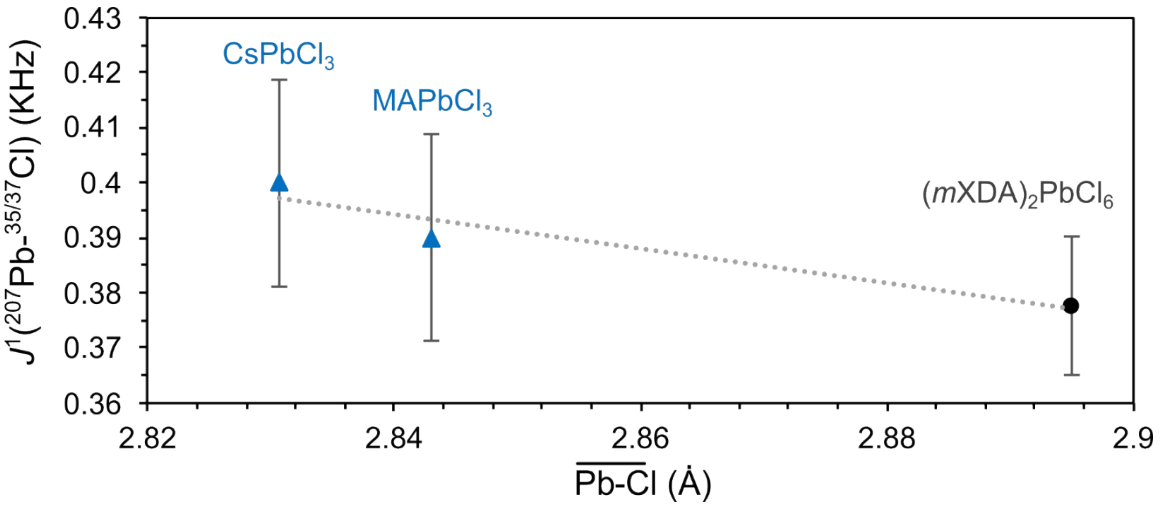

Figure S2. $^{207}Pb\text{-}^{35/37}Cl$ scalar coupling constants vs octahedral Pb-Cl mean atomic distance for the lead bromide perovskite series. A linear fit is presented with R^2 values of 0.923. Values taken from the report of Aebli *et al*. are marked with blue triangles.

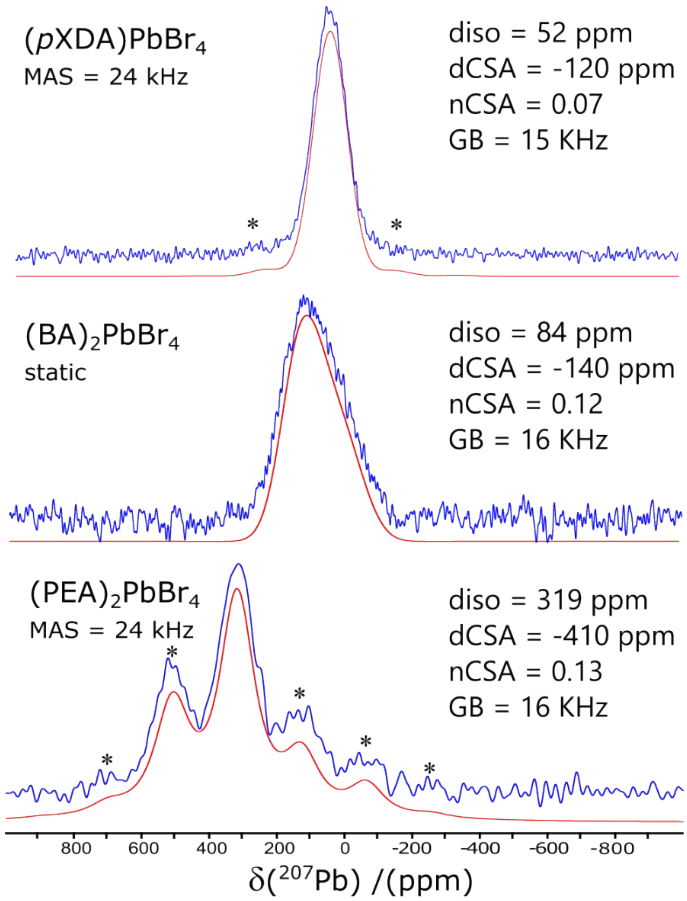

Figure S3. The ^{207}Pb NMR spectra of (pXDA)$PbBr_4$, $(BA)_2PbBr_4$, and $(PEA)_2PbBr_4$ fitted with chemical shift anisotropy (CSA) broadened resonances. CSA fitting parameters are displayed. Experimental spectra and simulated spectra are displayed in blue and red respectively. Spinning sidebands are marked by asterisks (*).

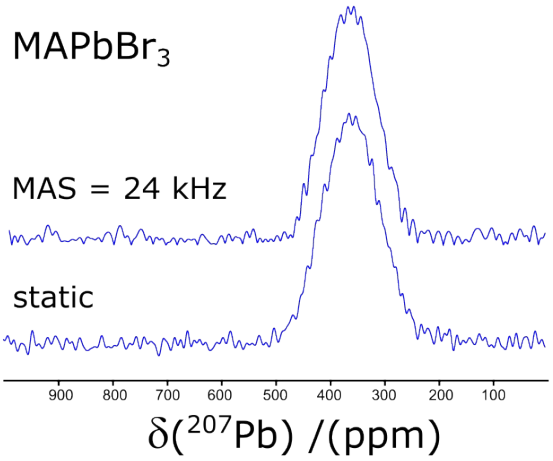

Figure S4. Comparison of the ^{207}Pb NMR spectra of $MAPbBr_3$ acquired under 24 kHz MAS and static conditions.

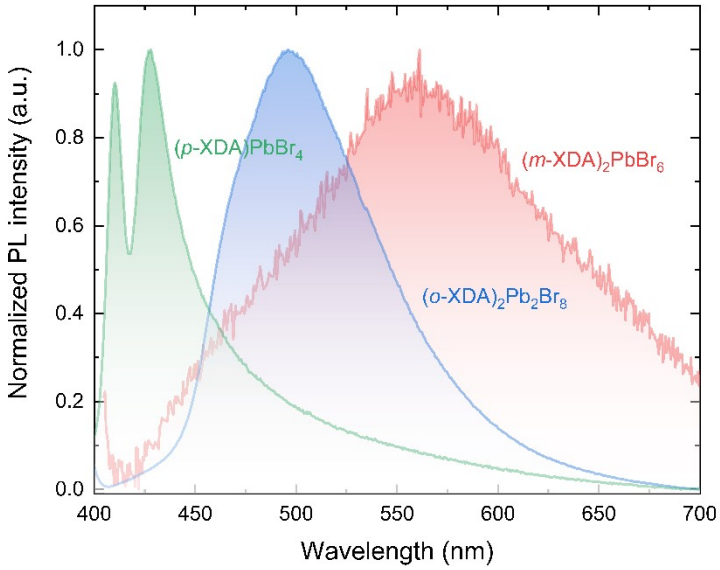

Figure S5. Photoluminescence spectra of $(o\text{XDA})_2Pb_2Br_8$, $(m\text{XDA})_2PbBr_6$, $(p\text{XDA})PbBr_4$ recorded upon excitation with UV light of 365 nm.

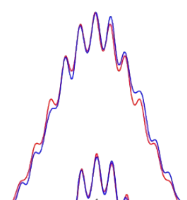

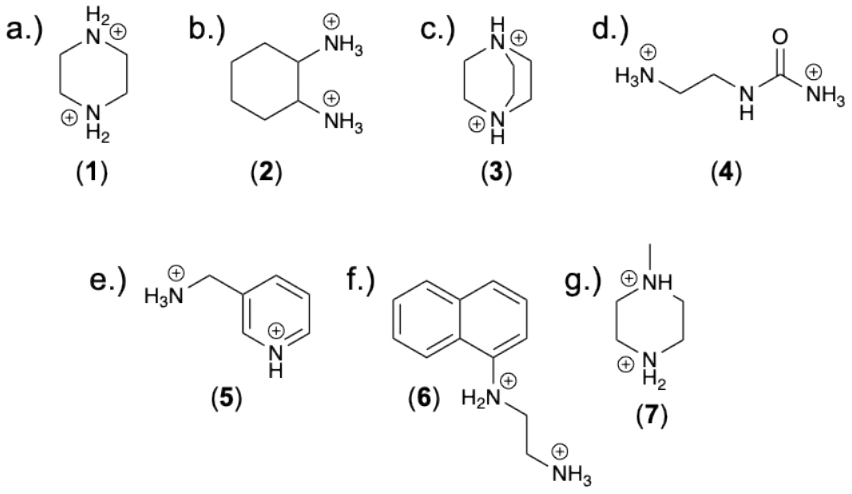

Figure S7. Molecular structures of organic cations capable of templating monomeric 0D $[PbBr_6]^{4-}$ structures reported in the literature.[2–8]

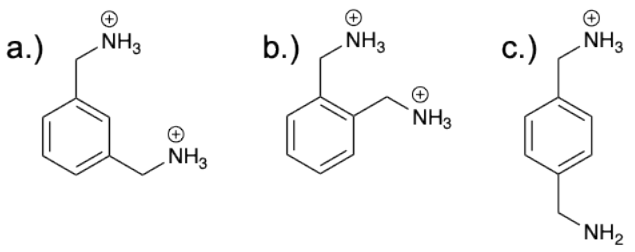

Figure S8. Molecular structures of different isomers of xylylenediammonium cations investigated in this study.

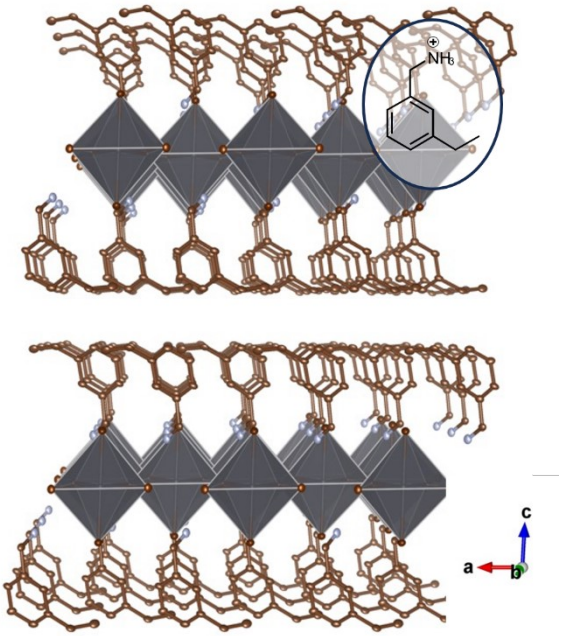

Figure S9. Single crystal X-ray structure of 2D perovskite templated by 3-ethylbenzylammonium. The inset shows the molecular structure of organic cation. Gray, maroon, brown, and blue spheres represent Pb, Br, C, and N atoms, respectively. H atoms are omitted for clarity. Ellipsoids are shown at 50% probability.

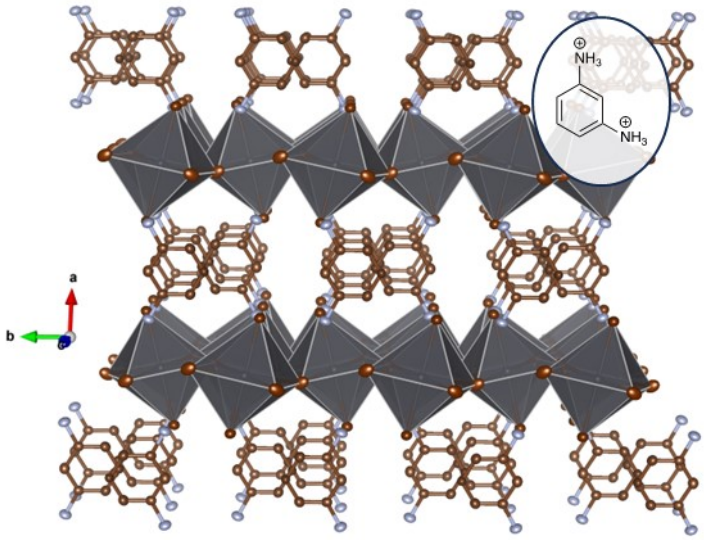

Figure S10. Single crystal X-ray structure of 2D perovskite templated by benzene-1,3-diaminium.[10] The inset shows the molecular structure of organic cation. Gray, maroon, brown, and blue spheres represent Pb, Br, C, and N atoms, respectively. H atoms are omitted for clarity. Ellipsoids are shown at 50% probability.

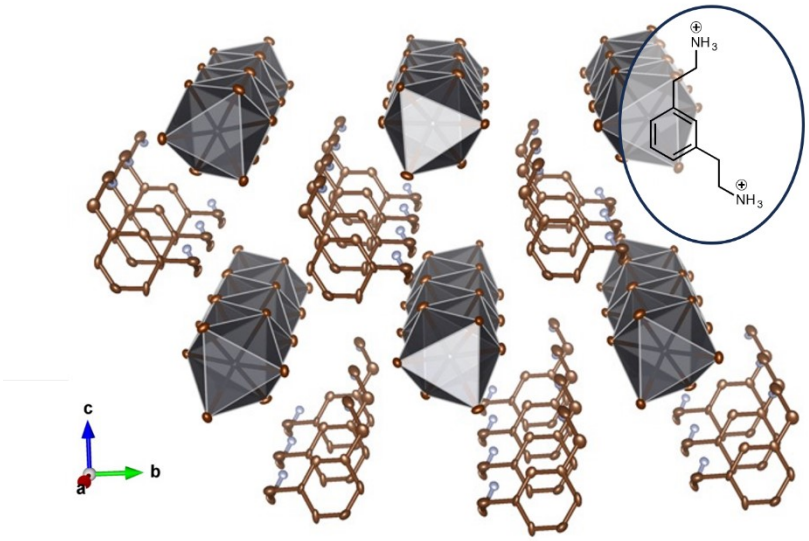

Figure S11. Single crystal X-ray structure of 1D perovskite templated by 2,2'-(1,3-phenylene)bis(ethan-1-aminium). The inset shows the molecular structure of organic cation. Gray, maroon, brown, and blue spheres represent Pb, Br, C, and N atoms, respectively. H atoms are omitted for clarity. Ellipsoids are shown at 50% probability.

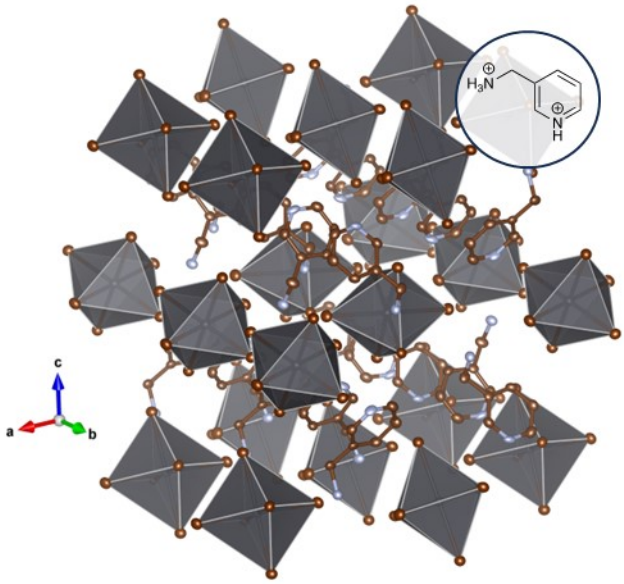

Figure S12. Single crystal X-ray structure of 0D perovskite templated by 3-(ammoniomethyl)pyridin-1-ium.[6] The inset shows the molecular structure of organic cation. Gray, maroon, brown, and blue spheres represent Pb, Br, C, and N atoms, respectively. H atoms are omitted for clarity. Ellipsoids are shown at 50% probability.

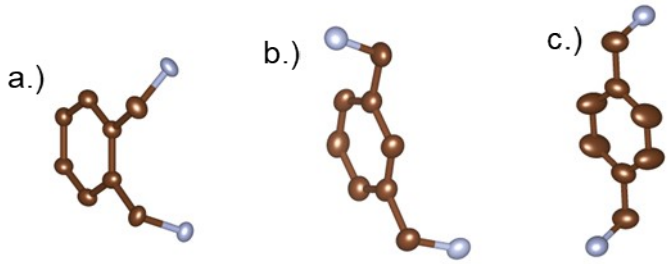

Figure S13. Structural conformations of organic dications a.) *ortho*-xylylenediammonium, b.) *meta*-xylylenediammonium, and c.) *para*-xylylenediammonium in the lattices of $(o\text{XDA})_2Pb_2Br_8$, $(m\text{-XDA})_2PbBr_6$, and $(p\text{XDA})PbBr_4$, respectively. Unlike those in b.) and c.), both ammonium groups in a.) point to the same directions. Brown and blue spheres represent C and N atoms, respectively. H atoms are omitted for clarity. Ellipsoids are shown at 50% probability.

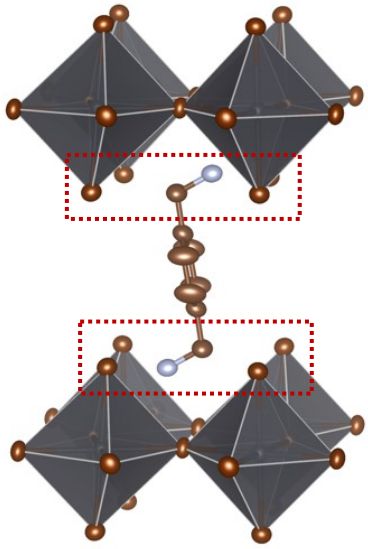

Figure S14. Formation of "bay area" (highlighted in red boxes) of the 2D perovskite $(p\text{XDA})PbBr_4$.

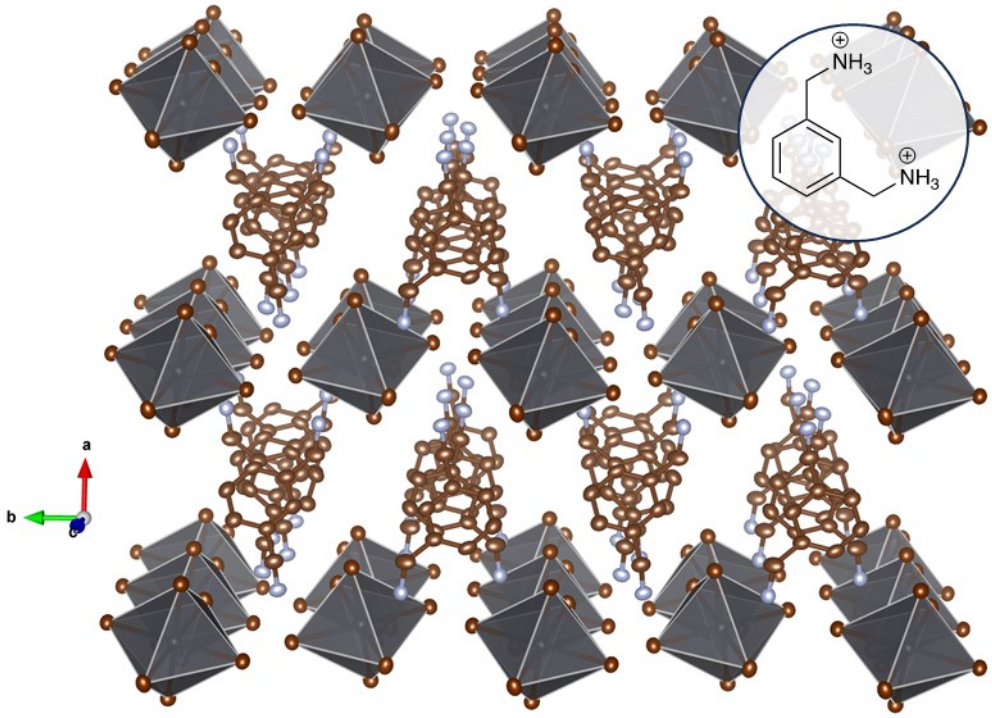

Figure S15. Single crystal X-ray structure of 0D perovskite templated by *meta*-xylylenediammonium showing alternating "layers" of organic and inorganic components along the *a* axis. Gray, maroon, brown, and blue spheres represent Pb, Br, C, and N atoms, respectively. H atoms are omitted for clarity. Ellipsoids are shown at 50% probability.

II. Supplementary note on low-dimensional perovskite cation templating

(*m*XDA)$_2$PbBr$_6$ is a rare example of "zero-dimensional" (0D) lead-bromide hybrid in which the inorganic component exists in the form of molecular $[PbBr_6]^{4-}$ ions. Such monomeric bromoplumbate configuration resembles that of 0D Cs_4PbBr_6 perovskite. Therein, each octahedron is surrounded and separated by the templating counter cations.[1] In total, there are less than ten compounds adopting the same inorganic motif reported in the literature.[2–10] The corresponding organic species responsible for directing the isolated lead-bromide octahedra formation are found to be diverse in structure and not related to each other (Figure S7(a-g)). This is partly because, unlike those in 2D perovskites, factors affecting the formability of 0D bromoplumbate are relatively unknown and systematic study to investigate such relationship is currently almost non-existent. Nonetheless, some similarities can still be observed from the aforementioned series of cations. These include the presence of both dicationic center and bulky core surrounding the ammonium groups within the organic structures. In this note, we attempt to delve further into those aspects by using the structural features of *m*XDA molecule (Figure S8(a)) as the focus of discussion. By doing so, we also aim to explain the rationale of judiciously selecting *m*XDA in this study, which allows the NMR spectroscopy properties of the resulting 0D halometallate motif to be probed.

First of all, the two ammonium groups in *m*XDA act as directing agents that drive the formation of the overall material lattices. This is achieved through various intermolecular interactions with the nearby lead-bromide octahedra (nearest N···I ranging from 3.342 to 3.464 Å). Each ammonium interacts with different octahedra whose physical separation is enforced by the

presence of the phenyl ring located at the center of the organic structure. This creates an isolation among the neighboring inorganic ions. To satisfy the charge balancing requirement, a $[PbBr_6]^{4-}$ is surrounded by four $[NH_3]^+$ and in the case of (*m*-XDA)$_2$PbBr$_6$, each $[NH_3]^+$ originates from four different *m*-XDA molecules. Such configuration is the most common among all other examples of 0D lead-bromide hybrids with the exception of compound in from Chen *et al.*[7] Therein, both positively-charged functionalities of cation (**6**) bind to the same $[PbBr_6]^{4-}$ moiety, creating a situation where one inorganic octahedron is surrounded by two organic molecules. We confirm that double cationic centers are needed for the bromoplumbate monomers formation. Replacing *m*-XDA with 3-ethylbenzylammonium species (Figure S9) resulted in a 2D perovskite despite the similarity in the steric profile between the ethyl- and methylammonium- functionalities. We reason that, being charged neutral, the former is incapable of providing the putative Coulombic interaction required to template the $[PbBr_6]^{4-}$ ions.

The exact length of the alkyl chain linker within the organic structure also proves to be important. In particular, only methylene group could lead to the 0D lead-bromide configuration (Figure 1(a)). Attaching ammonium functionalities directly onto the phenyl ring yielded a 2D perovskite with layered bromplumbate lattices (Figure S10). On the other hand, extending the linker by one carbon (*i.e.,* ethylene group) resulted in a hybrid material with 1D inorganic chain architectures (Figure S11). The essential presence and particularity of the methylene chain is further instantiated by the case of cation (**5**). Therein, although one methylammonium pendant is replaced with a pyridinium functionality, the presence of the remaining same pendant still afforded 0D monomeric $[PbBr_6]^{4-}$ motif in the final material (Figure S12). While further research and more examples are needed to explain the above observation more fully, we hypothesize that methylammonium moiety possesses the right degree of steric and flexibility profiles, all of which are required to accommodate the formation of isolated lead-bromide octahedra.

A very specific templating condition is further illustrated in the relative position of the methylammonium group, of which if not fulfilled, would result in the formation of different inorganic lattices. As presented in the main article, isomeric *o*XDA and *p*XDA cations (Figure S8(b-c)) led to hybrids with 1D and 2D lead-bromide frameworks, respectively (Figure 1(b-c)). The former occurred as the consequence of the relative distance of the two methylammoniums that are too near to one another. Such close proximity prohibited each of the groups to direct the creation of two independent $[PbBr_6]^{4-}$ octahedra whose nearest positions are allowable from Coulombic stand point. The fact that the methylammonium chain points to the same direction also makes the situation more unfavorable for the monomeric 0D lead-bromide to form (Figure S13). Thus, the most thermodynamically preferred structure to be templated under that situation is the 1D type. Meanwhile, the distance between the two methylammoniums is too far in the case of *p*XDA. While it is not suitable for the construction of 0D species, the structural feature of *p*XDA is actually fulfilling the requirement for 2D perovskite as the cationic centers are now isolated from each other and not sterically hindered.[9] This allows one bromoplumbate octahedron to corner-share with other four octahedral neighbors along an equatorial plane (relative to the Pb^{2+} metal center). Propagation in two directions eventually leads to layered $[PbBr_4]^{-2}$ architectures where a collection of bay regions (areas defined by the four nearest dangling bromide ligands) are resulted at the axial positions (Figure S14).

Steric bulk of the phenyl ring in *m*-XDA, coupled with the way the methylammonium functionalities interact with the bromoplumbate ions, causes asymmetry or unequal distribution in the overall materials packing of (*m*XDA)$_2$PbBr$_6$. In particular, there appears alternating "layers" of organic and inorganic components along the *a* axis of the hybrid's crystal structure (Figure S15). This configuration is a reminiscent of 2D perovskite and causes the distance of neighboring $[PbBr_6]^{4-}$ octahedra to be heavily axis-dependent. Typically, the inter octahedra distances are smallest along the *b* and *c* axes (Pb···Pb = 8.420 Å and Pb···Pb = 8.547 Å, respectively) due to the absence of the organic species "separators" and is biggest along the *a* axis (Pb···Pb = 10.744 Å). This is not a typical characteristic of this class of compound and it deviates quite a lot from that in Cs_4PbBr_6 where relatively similar inter octahedra distances (nearest Pb···Pb is *ca.* 8.431 Å) and more equal distribution of

the cationic charge center (in this case provided by Cs^+) can be found. Comparing this feature across the series of the published 0D lead-bromide materials, it is observed that organic cations with relatively small size would lead to inter octahedra distances that are similar to that in Cs_4PbBr_6,[2,4,8] while the bigger counterparts tend to follow (*m*-XDA)$_2PbBr_6$.[5–7] It is expected that more examples of 0D lead-bromide hybrids could contribute to the generalization of the templating pattern as well as formulation of a "design rule" for this class of materials.

Despite the specificity towards the choice of organic species, the materials' overall structures are observed to be more tolerant to the change in the inorganic components. Isovalent substitutions carried out on the Pb^{2+} metal center (to Sn^{2+}) and/or the Br^- ligand (to Cl^- and I^-) in (*m*XDA)$_2PbBr_6$ afforded materials with the same structural motifs and conformations. The most notable difference observed was the extent of hydrogen bonding interaction between the organic cation and anionic metal halide $[MX_6]^{4-}$ octahedra in the lattices, as indicated by the nearest N···X distances. Across the series of different 0D perovskites templated by *m*XDA, it is found that halometallate ions with smaller atoms would experience stronger interaction with the organic species relative to the those with bigger atoms (nearest N···Cl ranges from 3.185 to 3.245 Å in (*m*XDA)$_2SnCl_6$, while N···I ranges from 3.546 to 3.691 Å in (*m*XDA)$_2PbI_6$). The complete list of N···X atomic distances of different *m*-XDA-based compounds is presented in Table S4.

III. Supplementary tables

	Compound		
	(*m*XDA)$_2$PbBr$_6$	**(*o*XDA)$_2$Pb$_2$Br$_8$**	**(*p*XDA)PbBr$_4$**
Empirical formula	$C_{16}H_{28}Br_6N_4Pb$	$C_{16}H_{28}Br_8N_4Pb_2$	$C_8H_{14}Br_4N_2Pb$
Formula weight, g mol^{-1}	963.07 g/mol	1330.08 g/mol	665.04 g/mol
Temperature, K	296(2) K	100(2) K	296(2) K
Wavelength, Å	0.71073 Å	0.71073 Å	0.71073 Å
Crystal size, mm^3	0.020 x 0.040 x 0.060 mm	0.010 x 0.020 x 0.220 mm	0.020 x 0.040 x 0.100 mm
Crystal habit	colorless block	colorless needle	colorless block
Crystal system	monoclinic	monoclinic	monoclinic
Space group	P 1 21/c 1	P 1 21/c 1	P 1 21/c 1
Unit cell dimensions	*a* = 10.7441(12) Å	*a* = 14.3412(9) Å	*a* = 12.340(3) Å
	α = 90°	*α* = 90°	*α* = 90°
	b = 14.5106(17) Å	*b* = 25.4991(18) Å	*b* = 8.1590(15) Å
	β = 103.625(5)°	*β* = 94.616(3)°	*β* = 90.930(10)°
	c = 8.5473(12) Å	*c* = 8.1894(6) Å	*c* = 8.1725(19) Å

	γ = 90°	γ = 90°	γ = 90°
Volume, Å^3	1295.1(3) Å3	2985.0(4) Å^3	822.7(3) Å^3
Z	2	4	2
Density, g cm^{-3}	2.470 g/cm3	2.960 g/cm^3	2.685 g/cm^3
Absorption coefficient, mm^{-1}	15.780 mm-1	21.987 mm^{-1}	19.944 mm^{-1}
F(000)	888	2384	596
Theta range for data collection	2.40 to 32.61°	2.14 to 27.89°	2.99 to 33.71°
Index ranges	-16<=h<=15, -22<=k<=21, -12<=l<=11	-18<=h<=18, -33<=k<=29, -10<=l<=7	-19<=h<=19, -11<=k<=12, -12<=l<=12
Reflections collected	19517	31516	13687
Independent reflections	4727 [R(int) = 0.0995]	7105 [R(int) = 0.0713]	3280 [R(int) = 0.0575]
Coverage of independent reflections	99.90%	99.70%	99.80%
Absorption correction	Multi-Scan	Multi-Scan	Multi-Scan
Max. and min. transmission	0.74 and 0.14	0.81 and 0.16	0.69 and 0.15
Function minimized	$\Sigma\, w(F_o^2 - F_c^2)^2$	$\Sigma\, w(F_o^2 - F_c^2)^2$	$\Sigma\, w(F_o^2 - F_c^2)^2$
Data / restraints / parameters	4727 / 0 / 114	7105 / 0 / 275	3280 / 0 / 71
Goodness-of-fit on F^2	0.949	1.007	0.986
Δ/σ_{max}	0.001	0.002	0.001
Final *R* indices	2939 data	5640 data	2179 data
[$I > 2\sigma(I)$]	*R1* = 0.0515, *wR2* = 0.1152	*R1* = 0.0378, *wR2* = 0.0859	*R1* = 0.0379, *wR2* = 0.0746
R indices [all data]	*R1* = 0.0955, *wR2* = 0.1367	*R1* = 0.0530, *wR2* = 0.0939	*R1* = 0.0707, *wR2* = 0.0867
Largest diff. peak and hole, eÅ^{-3}	0.916 and -1.607	1.886 and -1.229	1.099 and -0.855
R.M.S. deviation from mean, eÅ^{-3}	0.265	0.243	0.166
CCDC code	2300670	2300671	2300669

Table S1. Crystallographic and structure refinement data for (*m*XDA)$_2$PbBr$_6$, (*o*XDA)$_2$Pb$_2$Br$_8$, and (*p*XDA)PbBr$_4$.[α]

[α]$R = \Sigma||F_o| - |F_c||/\Sigma|F_o|$, $wR = \{\Sigma[w(|F_o|^2 - |F_c|^2)^2]/\Sigma[w(|F_o|^4)]\}^{1/2}$ and (*m*-XDA)$_2$PbBr$_6$, $w = 1/[\sigma^2(F_o^2) + (0.0581P)^2]$; (*o*-XDA)$_2Pb_2Br_8$, $w = 1/[\sigma^2(F_o^2) + (0.0393P)^2]$; (*p*-XDA)PbBr$_4$, $w = 1/[\sigma^2(F_o^2) + (0.0322P)^2]$; where $P = (F_o^2 + 2F_c^2)/3$.

	Compound		
	(*m*XDA)$_2$PbCl$_6$	**(*m*XDA)$_2$SnCl$_6$**	**(*m*XDA)$_2$SnBr$_6$**
Empirical formula	$C_{16}H_{28}Cl_6N_4Pb$	$C_{16}H_{28}Cl_6N_4Sn$	$C_{16}H_{28}Br_6N_4Sn$
Formula weight, g mol^{-1}	696.31 g/mol	607.81 g/mol	874.57 g/mol
Temperature, K	100(2) K	100(2) K	296(2) K
Wavelength, Å	0.71073 Å	0.71073 Å	0.71073 Å
Crystal size, mm^3	0.005 x 0.040 x 0.060 mm	0.010 x 0.020 x 0.220 mm	0.020 x 0.040 x 0.100 mm
Crystal habit	colorless plate	colorless block	colorless block
Crystal system	monoclinic	monoclinic	monoclinic

Space group	P 1 21/c 1	P 1 21/c 1	P 1 21/c 1
Unit cell dimensions	a = 10.5772(11) Å	a = 10.5583(3) Å	a = 10.7578(3) Å
	α = 90°	α = 90°	α = 90°
	b = 13.8645(16) Å	b = 13.7185(4) Å	b = 14.4697(4) Å
	β = 102.816(4)°	β = 102.5760(10)°	β = 103.5453(14)°
	c = 8.2791(9) Å	c = 8.2248(3) Å	c = 8.5380(3) Å
	γ = 90°	γ = 90°	γ = 90°
Volume, Å^3	1183.9(2) Å^3	1162.73(6) Å^3	822.7(3) Å^3
Z	2	2	2
Density, g cm^{-3}	1.953 g/cm^3	1.736 g/cm^3	2.248 g/cm^3
Absorption coefficient, mm^{-1}	7.813 mm^{-1}	1.799 mm^{-1}	10.276 mm^{-1}
F(000)	672	608	824
Theta range for data collection	2.46 to 25.38°	2.47 to 36.41°	2.40 to 31.00°
Index ranges	-12<=h<=12, -16<=k<=16, -9<=l<=9	-17<=h<=17, -17<=k<=22, -10<=l<=13	-15<=h<=15, -20<=k<=20, -12<=l<=12
Reflections collected	16772	29976	13687
Independent reflections	20166 [R(int) = 0.0859]	5644 [R(int) = 0.0451]	4094 [R(int) = 0.0339]
Coverage of independent reflections	99.9%	99.50%	99.10%
Absorption correction	Multi-Scan	Multi-Scan	Multi-Scan
Max. and min. transmission factors	0.96 and 0.65	0.81 and 0.67	0.68 and 0.44
Function minimized	$\Sigma\, w(F_o^2 - F_c^2)^2$	$\Sigma\, w(F_o^2 - F_c^2)^2$	$\Sigma\, w(F_o^2 - F_c^2)^2$
Data / restraints / parameters	2166 / 0 / 126	5644 / 0 / 126	4094 / 0 / 126
Goodness-of-fit on F^2	1.059	1.088	1.033
Δ/σ_{max}	0.000	0.001	0.001
Final R indices	1953 data	5087 data	3340 data
[$I > 2\sigma(I)$]	$R1$ = 0.0388, $wR2$ = 0.1091	$R1$ = 0.0229, $wR2$ = 0.0489	$R1$ = 0.0281, $wR2$ = 0.0575
R indices [all data]	$R1$ = 0.0421, $wR2$ = 0.1134	$R1$ = 0.0276, $wR2$ = 0.0510	$R1$ = 0.0401, $wR2$ = 0.0605
Largest diff. peak and hole, eÅ^{-3}	1.519 and -1.792	0.546 and -0.929	1.044 and -0.977
R.M.S. deviation from mean, eÅ^{-3}	0.206	0.099	0.100
CCDC code	2350304	2300668	1545198

Table S2. Crystallographic and structure refinement data for (mXDA)$_2$PbCl$_6$, (mXDA)$_2$SnCl$_6$, and (mXDA)$_2$SnBr$_6$.[α]

[α] $R = \Sigma||F_o| - |F_c||/\Sigma|F_o|$, $wR = \{\Sigma[w(|F_o|^2 - |F_c|^2)^2]/\Sigma[w(|F_o|^4)]\}^{1/2}$ and (mXDA)$_2$PbCl$_6$, $w = 1/[\sigma^2(F_o^2) + (0.1818P)^2]$; ($m$XDA)$_2$SnCl$_6$, $w = 1/[\sigma^2(F_o^2) + (0.0151P)^2 + 0.3581P]$; ($m$XDA)$_2$SnBr$_6$, $w = 1/[\sigma^2(F_o^2) + (0.0225P)^2 + 0.8043P]$; where $P = (F_o^2 + 2F_c^2)/3$.

$(m\text{XDA})_2\text{PbI}_6$	$(m\text{XDA})_2\text{PbBr}_6$	$(m\text{XDA})_2\text{PbCl}_6$	$(m\text{XDA})_2\text{SnBr}_6$	$(m\text{XDA})_2\text{SnCl}_6$
3.546	3.418	3.205	3.376	3.185
3.573	3.370	3.206	3.41	3.197
3.603	3.464	3.228	3.462	3.204
3.552	3.342		3.348	3.209
3.644	3.354		3.365	3.212
3.691	3.384		3.384	3.245

Table S4. Nearest N···X distances as measured from the corresponding materials single crystal structure (Å)

Perovskites	Dimensionality	Space group	*B-X* length		*X-B-X* angle variance $^{\circ 2}$	$[BX_6]^{-4}$ eCoN [a]	Source
			Mean *Å*	σ *Å*			
$(m\text{XDA})_2\text{PbCl}_6$	0D	$Pm2_1/c$	2.895*(3)*	0.0147	33.76	5.995	[b]
$(m\text{XDA})_2\text{SnBr}_6$	0D	$Pm2_1/c$	2.9761*(3)*	0.0150	31.39	5.995	[b]
$(m\text{XDA})_2\text{SnCl}_6$	0D	$Pm2_1/c$	2.8602*(3)*	0.0140	33.05	5.995	[b]

Table S3. Structural parameters determined via SCXRD. Uncertainties are represented in italic parentheses.
[a] Effective coordination number
[b] Determined in this work

IV. References

1 M. De Bastiani, I. Dursun, Y. Zhang, B. A. Alshankiti, X.-H. Miao, J. Yin, E. Yengel, E. Alarousu, B. Turedi, J. M. Almutlaq, M. I. Saidaminov, S. Mitra, I. Gereige, A. AlSaggaf, Y. Zhu, Y. Han, I. S. Roqan, J.-L. Bredas, O. F. Mohammed and O. M. Bakr, *Chem. Mater.*, 2017, **29**, 7108–7113.

2 Y. Takeoka, K. Asai, M. Rikukawa and K. Sanui, *Chem. Lett.*, 2005, **34**, 602–603.

3 Y. Wei, C. Li, Y. Li, Z. Luo, X. Wu, Y. Liu, L. Zhang, X. He, W. Wang and Z. Quan, *Angewandte Chemie International Edition*, 2022, **61**, e202212685.

4 J.-L. Song, W.-J. Chen, K.-B. Chu and Y.-H. Zhou, *Dalton Trans.*, 2018, **47**, 14497–14502.

5 B.-B. Cui, Y. Han, B. Huang, Y. Zhao, X. Wu, L. Liu, G. Cao, Q. Du, N. Liu, W. Zou, M. Sun, L. Wang, X. Liu, J. Wang, H. Zhou and Q. Chen, *Nat Commun*, 2019, **10**, 5190.

6 Y. Li, G. Zheng, C. Lin and J. Lin, *Solid State Sciences*, 2007, **9**, 855–861.

7 Y. Chen, Y.-Y. Zheng, G. Wu, M. Wang, H.-Z. Chen and H. Yang, *Acta Crystallogr Sect E Struct Rep Online*, 2010, **66**, m417.

8 M.-H. Jung, K. C. Ko and W. R. Lee, *Dalton Trans.*, 2019, **48**, 15074–15090.

9 B. Saparov and D. B. Mitzi, *Chem. Rev.*, 2016, **116**, 4558–4596.

10 P. Fu, M. A. Quintero, C. Welton, X. Li, B. Cucco, M. C. De Siena, J. Even, G. Volonakis, M. Kepenekian, R. Liu, C. C. Laing, V. Klepov, Y. Liu, V. P. Dravid, G. N. Manjunatha Reddy, C. Li and M. G. Kanatzidis, *Chem. Mater.*, 2022, **34**, 9685–9698.